Article

Enhance the Optical Absorptivity of Nanocrystalline TiO Film with High Molar Extinction Coefficient Ruthenium Sensitizers for High Performance Dye-Sensitized Solar Cells

Feifei Gao, Yuan Wang, Dong Shi, Jing Zhang, Mingkui Wang, Xiaoyan Jing, Robin Humphry-Baker, Peng Wang, Shaik M. Zakeeruddin, and Michael Gra#tzel

J. Am. Chem. Soc., **2008**, 130 (32), 10720-10728 • DOI: 10.1021/ja801942j • Publication Date (Web): 22 July 2008

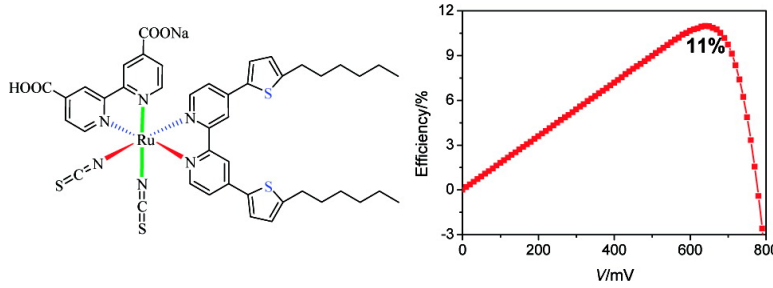

More About This Article

Additional resources and features associated with this article are available within the HTML version:

- Supporting Information
- Links to the 5 articles that cite this article, as of the time of this article download
- Access to high resolution figures
- Links to articles and content related to this article
- Copyright permission to reproduce figures and/or text from this article

View the Full Text HTML

J|A|C|S
ARTICLES

Published on Web 07/22/2008

Enhance the Optical Absorptivity of Nanocrystalline TiO_2 Film with High Molar Extinction Coefficient Ruthenium Sensitizers for High Performance Dye-Sensitized Solar Cells

Feifei Gao,[†] Yuan Wang,[†,‡] Dong Shi,[†] Jing Zhang,[†] Mingkui Wang,[⊥] Xiaoyan Jing,[‡] Robin Humphry-Baker,[⊥] Peng Wang,[*,†] Shaik M. Zakeeruddin,[*,⊥] and Michael Grätzel[*,⊥]

State Key Laboratory of Polymer Physics and Chemistry, Changchun Institute of Applied Chemistry, Chinese Academy of Sciences (CAS), Changchun 130022, China, Key Laboratory of Superlight Materials and Surface Technology, Harbin Engineering University, Harbin 150001, China, and Laboratory for Photonics and Interfaces, Swiss Federal Institute of Technology, CH 1015, Lausanne, Switzerland

Received March 15, 2008; E-mail: peng.wang@ciac.jl.cn; shaik.zakeer@epfl.ch; michael.graetzel@epfl.ch

Abstract: We report two new heteroleptic polypyridyl ruthenium complexes, coded C101 and C102, with high molar extinction coefficients by extending the π-conjugation of spectator ligands, with a motivation to enhance the optical absorptivity of mesoporous titania film and charge collection yield in a dye-sensitized solar cell. On the basis of this C101 sensitizer, several DSC benchmarks measured under the air mass 1.5 global sunlight have been reached. Along with an acetonitrile-based electrolyte, the C101 sensitizer has already achieved a strikingly high efficiency of 11.0−11.3%, even under a preliminary testing. More importantly, based on a low volatility 3-methoxypropionitrile electrolyte and a solvent-free ionic liquid electrolyte, cells have corresponding >9.0% and ~7.4% efficiencies retained over 95% of their initial performances after 1000 h full sunlight soaking at 60 °C. With the aid of electrical impedance measurements, we further disclose that, compared to the cell with an acetonitrile-based electrolyte, a dye-sensitized solar cell with an ionic liquid electrolyte shows a feature of much shorter effective electron diffusion lengths due to the lower electron diffusion coefficients and shorter electron lifetimes in the mesoporous titania film, explaining the photocurrent difference between these two type devices. This highlights the next necessary efforts to further improve the efficiency of cells with ionic liquid electrolytes, facilitating the large-scale production and application of flexible thin film mesoscopic solar cells.

Introduction

Elegant and benign photovoltaic (PV) cells generating clean electricity when illuminated by sunlight or artificial light are now poised for significant market expansion in this new millennium, considering that solar energy is the major renewable energy source apart from the depletion and pollution of fossil fuels.[1] It is widely recognized that the performance/price ratio will play a pivotal role in the future choice of various PV devices. In the past years, low-cost excitonic solar cells made from organic optoelectronic materials have received surging academic and industrial attentions as potential candidates for the future PV market.[2] In the family of organic photovoltaic devices, the mesoscopic dye-sensitized solar cell[3] (DSC) has achieved a respectable high efficiency[4] and a remarkable stability under the prolonged thermal and light-soaking dual stress.[5]

It is fair to note that until now the ~11% efficiency record[4] of DSCs measured under the air mass 1.5 global (AM 1.5G) illumination is kept with the well-known N719 or N749 sensitizer employing a thick mesoscopic titania film and a volatile acetonitrile-based electrolyte. However, stability under prolonged heating at 80 °C has proved too hard to reach with the high efficiency N719- or N749-based cells. In 2003, a thermally stable, ~7% efficiency DSC[5b] was disclosed, employing the amphiphilic Z907 sensitizer[5a] and a 3-methoxypropi-

[†] Changchun Institute of Applied Chemistry, CAS.
[‡] Harbin Engineering University.
[⊥] Swiss Federal Institute of Technology.

(1) Archer, M. D.; Hill, R. *Clean Electricity from Photovoltaics*; Imperical College Press: London, 2001.
(2) For a special issue on organic-based photovoltaics, see: *MRS Bull.* **2005**, *30*, 10–53.
(3) (a) O'Regan, B.; Grätzel, M. *Nature* **1991**, *353*, 737. (b) Grätzel, M. *Nature* **2001**, *414*, 338.
(4) (a) Nazeeruddin, M. K.; De Angelis, F.; Fantacci, S.; Selloni, A.; Viscardi, G.; Liska, P.; Ito, S.; Takeru, B.; Grätzel, M. *J. Am. Chem. Soc.* **2005**, *127*, 16835. (b) Chiba, Y.; Islam, A.; Watanabe, Y.; Komiya, R.; Koide, N.; Han, L. *Jpn. J. Appl. Phys., Part 2* **2006**, *45*, L638.
(5) (a) Wang, P.; Zakeeruddin, S. M.; Moser, J.-E.; Nazeeruddin, M. K.; Sekiguchi, T.; Grätzel, M. *Nat. Mater.* **2003**, *2*, 402. (b) Wang, P.; Zakeeruddin, S. M.; Humphry-Baker, R.; Moser, J.-E.; Grätzel, M. *Adv. Mater.* **2003**, *15*, 2101. (c) Wang, P.; Klein, C.; Humphry-Baker, R.; Zakeeruddin, S. M.; Grätzel, M. *J. Am. Chem. Soc.* **2005**, *127*, 808. (d) Wang, P.; Klein, C.; Humphry-Baker, R.; Zakeeruddin, S. M.; Grätzel, M. *Appl. Phys. Lett.* **2005**, *86*, 123508. (e) Kuang, D.; Klein, C.; Ito, S.; Moser, J.-E.; Humphry-Baker, R.; Evans, N.; Duriaux, F.; Grätzel, C.; Zakeeruddin, S. M.; Grätzel, M. *Adv. Mater.* **2007**, *19*, 1133.

10.1021/ja801942j CCC: $40.75

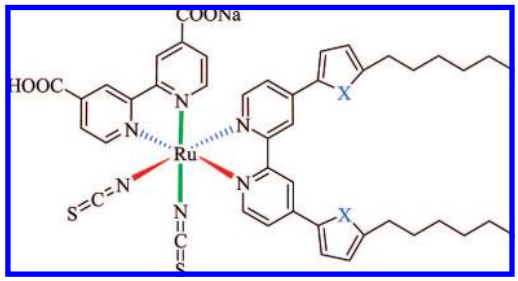

Figure 1. Molecular structures of the C101 (X = S) and C102 (X = O) sensitizers.

onitrile (MPN)-based electrolyte avoiding lithium salts as additives. We must remark that the always neglected latter point has also made a seminal contribution to realize thermostable DSCs. However, the molar extinction coefficient of this sensitizer is somewhat lower than that of the standard N719 dye. Meanwhile, a compromise between efficiency and high temperature stability has been noted for the Z907 sensitizer.[6] For commercial applications of DSCs, it is necessary to employ nonvolatile or even solvent-free electrolytes. However, with a low-fluidity electrolyte the charge collection yield becomes low due to the shortened electron diffusion length. Enhancing the optical absorptivity of a stained mesoporous film can counter this effect. Thus, we initiated the concept of developing high molar extinction coefficient, amphiphilic ruthenium sensitizer,[7] followed by other groups,[8] with a motivation to enhance device efficiency of DSCs. In this context, we have successfully developed sensitizers such as K19[5c,d] and its analogue K77[5e] to fabricate thermally stable DSCs showing ~8 and ~8.5% initial efficiencies, respectively. Unfortunately, with an acetonitrile-based electrolyte, all these recently reported sensitizers have not achieved a power conversion efficiency of 11% yet. Here we report a very promising sensitizer coded C101 and shown in Figure 1 to solve this dilemma, with which several new DSC benchmarks have been accomplished. Structures of other mentioned dyes are presented in Figure S1, Supporting Information. While our work was in progress, Wu *et al.*[8e] communicated a similar sensitizer like C101 with a molar extinction coefficient of 15.7×10^3 M^{-1} cm^{-1}, showing an efficiency of 7.39% with a highly volatile acetonitrile-based electrolyte.

Experimental Section

Materials. All solvents and reagents, unless otherwise stated, were of puriss quality and used as received. Thiophene, *n*-butyllithium, $[RuCl_2(p\text{-cymene})]_2$ and tetra-*n*-butylammonium hexafluorophosphate were purchased from Aldrich. Guanidinium thiocyanate (GNCS), 3α,7α-dihyroxy-5β-cholic acid (Cheno), *tert*-butylpyridine, and MPN were purchased from Fluka. Sephadex LH-20 was obtained from Pharmacia. 4,4′-Dicarboxylic acid-2,2′-bipyridine (dcbpy), 400 nm sized TiO_2 anatase particles, and 1-ethyl-3-methylimidazolium tetracyanoborate (EMITCB) were received as gifts from Nanjing Chemzam PharmTech Co., Catalysts & Chemical Ind. Co. (CCIC), and Merck, respectively. 1,3-Dimethylimidazolium iodide (DMII) and 1-ethyl-3-methylimidazolium iodide (EMII) were prepared according to the reported procedure[9] and their purities were confirmed by ^{1}H NMR analysis. *N*-Butylbenzimidazole (NBB) was synthesized according to the literature method[10] and distilled before use. 4,4′-Dibromo-2,2′-bipyridine[11] and 2-hexylfuran[12] were synthesized according to the literature methods.

Synthesis of 2-Hexylthiophene. To a stirred solution of thiophene (10.00 g, 0.12 mol) in anhydrous CH_2Cl_2 (100 mL) was added hexanoyl chloride (17.20 mL, 0.13 mol). The mixture was stirred for 30 min at room temperature and then cooled to 0 °C, and $AlCl_3$ (20.62 g, 0.16 mol) was added portionwise. The mixture was warmed to 25 °C and stirred overnight. The reaction was quenched by the addition of water and acidified with 2 M HCl aqueous solution. The mixture was extracted with CH_2Cl_2. The organic layer was washed with water and dried over $MgSO_4$. After removing solvent, the crude product was purified by column chromatography (CH_2Cl_2/*n*-hexane: 1/1) on silica gel to afford 1-(thiophen-2-yl)-hexan-1-one (15.70 g, 72% yield) as a colorless liquid. ^{1}H NMR (600 MHz, $CDCl_3$, δ_H): 7.71 (d, J = 4.0 Hz, 1H), 7.62 (d, J = 4.0 Hz, 1H), 7.12 (t, J = 4.0 Hz, 1H), 2.89 (t, J = 8.0 Hz, 2H), 1.77−1.74 (m, 2H), 1.35−1.37 (m, 4H), 0.91 (t, J = 8.0 Hz, 3H). $LiAlH_4$ (22.37 g, 0.590 mol) and $AlCl_3$ (18.67 g, 0.14 mol) were separately added to cold anhydrous ether (200 mL) slowly and the resulting suspended solutions were carefully mixed. To this mixture was added 1-thiophen-2-yl-hexan-1-one (11.0 g, 0.06 mol) in dry ether at 0 °C. The mixture was warmed to room temperature and then stirred for 3 h. The reaction was quenched by the careful addition of ether and 2 M HCl aqueous solution. The gray precipitate was filtered off and washed with ether. The combined filtrate was extracted, washed with water, and dried over $MgSO_4$. After rotary evaporation of solvent, the crude product was purified with column chromatography (*n*-hexane) on silica gel to afford a colorless liquid (8.94 g, 89% yield). ^{1}H NMR (600 MHz, $CDCl_3$, δ_H): 7.10 (dd, J = 5.2 Hz, J = 1.2 Hz, 1H), 6.91 (q, 1H), 6.83 (dd, J = 3.3 Hz, J = 0.9 Hz, 1H), 2.82 (t, J = 7.8 Hz, 2H), 1.69−1.53 (m, 2H), 1.38−1.28 (m, 6H), 0.88 (t, J = 6.8 Hz, 3H).

Synthesis of 4,4′-Bis(5-hexylthiophen-2-yl)-2,2′-bipyridine (L1). *n*-Butyllithium (11.40 mL, 2.5 M in hexane, 2.85 mmol) was added dropwise to a solution of 2-hexylthiophene (4.00 g, 2.38 mmol) in anhydrous THF at −78 °C under Ar. The mixture was stirred at this temperature for 30 min and then for 1.5 h at room temperature, and after cooling to −78 °C, tributylstannyl chloride (10.06 g, 3.09 mmol) was added. After stirring for 4 h at room temperature, the reaction was terminated by adding saturated NH_4Cl aqueous solution. The mixture was extracted with CH_2Cl_2 and dried over $MgSO_4$. After the removal of solvent, the crude 2-hexyl-5-tributylstannylthiophene (8.74 g, 19.11 mmol) was mixed with 4,4′-dibromo-2,2′-bipyridine (2.00 g, 6.37 mmol) in 220 mL of DMF. The catalyst $Pd(PPh_3)_2Cl_2$ (0.25 g, 0.32 mmol) was added to the solution and the mixture was stirred at 85 °C under Ar overnight. After rotary evaporation of DMF, the resulting solid was purified by column chromatography on silica gel using $CHCl_3$ as eluent to afford **L1** (2.49 g, 80% yield) as ivory white solid. ^{1}H NMR (600 MHz, $CDCl_3$, δ_H): 8.63 (d, J = 5.4 Hz, 2H), 8.60 (s, 2H), 7.49 (d, J = 3.0 Hz, 2H), 7.45 (d, J = 4.8 Hz, 2H), 6.82 (d, J = 3.0 Hz, 2H), 2.85 (t, J = 5.0 Hz, 4H), 1.74−1.69 (m, 4H), 1.41−1.32 (m, 12H), 0.90 (t, J = 6.6 Hz, 6H). MS (EI) *m*/*z* calcd for ($C_{30}H_{36}N_2O_2$), 488.75; found, 488.

(6) Durrant, J. R.; Haque, S. A. *Nat. Mater.* **2003**, *2*, 362.
(7) Wang, P.; Zakeeruddin, S. M.; Moser, J.-E.; Humphry-Baker, R.; Comte, P.; Aranyos, V.; Hagfeldt, A.; Nazeeruddin, M. K.; Grätzel, M. *Adv. Mater.* **2004**, *16*, 1806.
(8) (a) Jiang, K.-J.; Masaki, N.; Xia, J.-B.; Noda, S.; Yanagida, S. *Chem. Commun.* **2006**, 2460. (b) Jang, S.-R.; Lee, C.; Choi, H.; Ko, J. J.; Lee, J.; Vittal, R.; Kim, K.-J. *Chem. Mater.* **2006**, *18*, 5604. (c) Chen, C.-Y.; Wu, S.-J.; Wu, C.-G.; Chen, J.-G.; Ho, K.-C. *Angew Chem., Int. Ed.* **2006**, *45*, 5822. (d) Karthikeyan, C. S.; Wietasch, H.; Thelakkat, M. *Adv. Mater.* **2007**, *19*, 1091. (e) Chen, C.-Y.; Wu, S.-J.; Li, J.-Y.; Wu, C.-G.; Chen, J.-G.; Ho, K.-C. *Adv. Mater.* **2007**, *19*, 3888.
(9) Bonhôte, P.; Dias, A.-P.; Armand, M.; Papageorgiou, N.; Kalyanasundaram, K.; Grätzel, M. *Inorg. Chem.* **1996**, *35*, 1168.
(10) Pilarski, B. *Liebigs Ann. Chem.* **1983**, 1078.
(11) (a) Maerker, G.; Case, F. H. *J. Am. Chem. Soc.* **1958**, *80*, 2745. (b) Wenkert, D.; Woodward, R. B. *J. Org. Chem.* **1983**, *48*, 283.
(12) Sheu, J.-H.; Yen, C.-F.; Huang, H.-C.; Hong, Y.-L. V. *J. Org. Chem.* **1989**, *54*, 5126.

Synthesis of 4,4′-Bis(5-hexylfuran-2-yl)-2,2′-bipyridine (L2). 2-Hexylfuran (2.20 g, 14.45 mmol) was dissolved in 40 mL of anhydrous THF and cooled to −78 °C. After addition of *n*-butyllithium (6.90 mL, 2.5 M in hexane, 17.34 mmol), the solution was stirred under Ar at −78 °C for 1 h. The mixture was stirred for 3 h at 20 °C and then cooled to −78 °C. Tributylstannyl chloride (6.12 g, 18.80 mmol) in 10 mL of anhydrous THF was added dropwise via a syringe and stirred for 2 h at −78 °C. The mixture was stirred overnight at room temperature. The reaction mixture was quenched with aqueous NH_4Cl and extracted with CH_2Cl_2. The combined organic layers were dried over $MgSO_4$. After the removal of solvent, the unpurified 2-hexyl-5-tributylstannylfuran (4.22 g, 9.55 mmol) and 4,4′-dibromo-2,2′-bipyridine (1.00 g, 3.18 mmol) were dissolved in 120 mL of DMF. A catalytic amount of $Pd(PPh_3)_2$ Cl_2 (0.13 g, 0.16 mmol) was added and the reaction mixture was stirred at 85 °C under Ar overnight. After the removal of DMF, the resulting solid was passed through a silica gel column using $CHCl_3$ as eluent to afford **L2** (1.12 g, 77% yield) as yellowish solid. ^{1}H NMR (600 MHz, $CDCl_3$, δ_H): 8.66 (dd, J = 5.2 Hz, J = 0.6 Hz, 2H), 8.61 (s, 2H), 7.54 (dd, J = 5.2 Hz, J = 1.6 Hz, 2H), 6.93 (d, J = 2.8 Hz, 2H), 6.13 (d, J = 3.2 Hz, 2H), 2.72 (t, J = 7.6 Hz, 4H), 1.75−1.67 (m, 4H), 1.44−1.31 (m, 12H), 0.90 (t, J = 7.0 Hz, 6H). MS (EI) m/z calcd for ($C_{30}H_{36}N_2O_2$), 456.62; found, 456.

Synthesis of NaRu(4,4′-bis(5-hexylthiophen-2-yl)-2,2′-bipyridine)(4-carboxylic acid-4′-carboxylate-2,2′-bipyridine)(NCS)$_2$ (C101). Dichloro(*p*-cymene)ruthenium(II) dimmer (0.32 mmol) and **L1** (0.64 mmol) were dissolved in DMF. The reaction mixture was stirred at 80 °C for 4 h under Ar in the dark. Subsequently, 4,4′-dicarboxylic acid-2,2′-bipyridine (0.64 mmol) was added into the flask and the reaction mixture was stirred at 140 °C for 4 h. At last, an excess of NH_4NCS (26.50 mmol) was added to the resulting dark solution and the reaction continued for another 4 h at the same temperature. Then the reaction mixture was cooled down to room temperature and the solvent was removed on a rotary evaporator under vacuum. Water was added to get the precipitate. The solid was collected on a sintered glass crucible by suction filtration, washed with water and Et_2O, and dried under vacuum. The crude complex was dissolved in basic methanol (NaOH) and purified on a Sephadex LH-20 column with methanol as eluent. The collected main band was concentrated and slowly dropped with an acidic methanol solution (HNO_3) to pH 5.9. Yield with column purification (4×): 63%. The precipitate was collected on a sintered glass crucible by suction filtration and dried in air. ^{1}H NMR (200 MHz, CD_3OD+NaOD, δ_H): 9.65 (d, 1H), 9.10 (d, 1H), 9.00 (s, 1H), 8.85 (s, 1H), 8.40 (s, 1H), 8.35 (d, 1H), 8.25 (s, 1H), 8.10 (d, 1H), 7.95 (d, 1H), 7.65 (d, 1H), 7.55 (d, 1H), 7.45 (d, 1H), 7.10−7.20 (m, 3H), 6.85 (d, 1H), 3.05 (t, 2H), 2.95 (t, 2H), 1.80 (m, 4H), 1.50 (m, 12H), 1.00 (m, 6H). Anal. Calcd for $NaRuC_{44}H_{43}N_6O_4S_4\cdot 2H_2O$: C, 52.42; H, 4.70; N, 8.34%. Found: C, 52.53; H, 4.68; N, 8.19%.

Synthesis of NaRu(4,4′-bis(5-hexylfuran-2-yl)-2,2′-bipyridine)(4-carboxylic acid-4′-carboxylate-2,2′-bipyridine)(NCS)$_2$ (C102). The synthesis and column purification were done with the same procedures described above for C101. After collecting the main band and rotary evaporating the solvent, the resultant solid was redissolved in water. Lowering the pH to 4.8 by titration with dilute nitric acid afforded a precipitate. The precipitate was collected on a sintered glass crucible by suction filtration and dried in air. Yield with column purification (4×): 60%. ^{1}H NMR (200 MHz, CD_3OD+NaOD, δ_H): 9.65 (d, 1H), 9.05 (d, 1H), 9.00 (s, 1H), 8.80 (s, 1H), 8.35 (d, 1H), 8.15 (s, 1H), 8.00 (s, 1H), 7.60−7.50 (m, 4H), 7.40 (d, 1H), 7.00 (d, 1H), 6.80 (d, 1H), 6.50 (d, 1H), 6.40 (d, 1H), 3.05 (t, 2H), 2.85 (t, 2H), 1.80 (m, 4H), 1.50 (m, 12H), 1.05 (m, 6H). Anal. Calcd for $NaRuC_{44}H_{43}N_6O_6S_2\cdot 4H_2O$: C, 52.22; H, 5.08; N, 8.30%. Found: C, 52.50; H, 4.97; N, 8.09%.

Calculation Methods. To get insight on the geometric structures and electronic transition properties of the C101 and C102 sensitizers viewed from the molecular orbital level, we performed density functional theory (DFT) and time dependent density functional theory (TDDFT) calculations in the Gaussian03 program package, with B3LYP/3-21G* functional and basis set.[13] In both C101 and C102 complexes, the central ruthenium (II) atom adopts a low spin $4d^6 5s^0$ electronic configuration in the quasi-octahedral symmetrical ligand field.[14] Based on such a model, we optimized their geometrical structures and further calculated the lowest 60 singlet−singlet transitions. Without any symmetry constraints, the geometry was optimized in vacuo and solvent effects of acetontrile were included in TDDFT calculation by means of the Polarizable Continuum Model.[15] On the basis of TDDFT results, we calculated in SWizard program (http://www.sg-chem.net/swizard/) the absorption profile as a sum of Gaussian band using the following equation[16]

$$\varepsilon(\omega) = 2.174\times 10^9 \sum_I \frac{f_I}{\Delta_{1/2,I}} \exp\left(-2.773\frac{(\omega-\omega_I)^2}{\Delta_{1/2,I}^2}\right) \qquad (1)$$

where ε is the molar extinction coefficient given in units of M^{-1} cm^{-1}, the energy ω of all allowed transitions included in eq 1 is expressed in cm^{-1}, f_I denotes the oscillator strength, and the half-bandwidths, $\Delta_{1/2}$, are assumed to be 3000 cm^{-1}.

UV−Vis, Emission, and Voltammetric Measurements. Electronic absorption spectra were performed on a Cary 5 spectrophotometer. Emission spectra were recorded with a Spex Fluorolog 112 spectrofluorometer. The emitted light was detected with a Hamamatsu R2658 photomultiplier operated in a single-photon counting mode. The emission spectra were photometrically corrected with a calibrated 200 W tungsten lamp as reference source. A computer controlled CHI 660C electrochemical workstation was used for square-wave voltammetric measurements in combination with a mini electrochemical cell equipped with a 5 μm radius Pt ultramicroelectrode as the working electrode. A Pt wire and a silver wire were used as counter- and quasi-reference electrodes, respectively. The redox potential values versus the ferrocene internal reference were converted to those versus NHE (normal hydrogen electrode).

ATR-FTIR Measurements. ATR-FTIR spectra were measured using a FTS 7000 FTIR spectrometer (Digilab, USA). The data reported here were taken with the "Golden Gate" diamond anvil ATR accessory. Spectra were derived from 64 scans at a resolution of 2 cm^{-1}. The samples were measured under the same mechanical force pushing the samples in contact with the diamond window. No ATR correction has been applied to the data. It also has to be appreciated that this ATR technique probes at most 1 μm of sample depth and that this depends on the sample refractive index, porosity etc. Some of the spectra show artifacts due to attenuation of light by the diamond window in the 2000 to 2350 cm^{-1} region. Dye-coated films were rinsed in acetonitrile and dried prior to measuring the spectra.

Device Fabrication. A screen-printed double layer film of interconnected TiO_2 particles was used as mesoporous negative electrode. A 7 μm thick film of 20 nm sized TiO_2 particles was first printed on the fluorine-doped SnO_2 conducting glass electrode and further coated by a 5 μm thick second layer of 400-nm-sized light scattering anatase particles. The detailed preparation procedures of TiO_2 nanocrystals, pastes for screen-printing, and double-layer nanostructured TiO_2 film have been reported in our previous paper.[17] Unless otherwise stated with cheno as coadsorbent, a TiO_2 electrode was stained by immersing it into a dye solution containing 300 μM of C101 or C102 sensitizer in the mixture of acetonitrile and *tert*-butanol (volume ratio: 1/1) overnight. After washing with

(13) (a) Becke, A. D. *J. Chem. Phys.* **1993**, *98*, 5648. (b) Lee, C.; Yang, W.; Parr, R. G. *Phys. Rev. B* **1988**, *37*, 785.
(14) Pourtois, G.; Beljonne, D.; Moucheron, C.; Schumm, S.; Mesmaeker, A. K.; Lazzaroni, R.; Brédas, J. L. *J. Am. Chem. Soc.* **2004**, *126*, 683.
(15) Foresman, J. B.; Keith, T. A.; Wiberg, K. B.; Snoonian, J.; Frisch, M. J. *J. Phys. Chem.* **1996**, *100*, 16098.
(16) Hay, P. J.; Wadt, W. R. J. *J. Chem. Phys.* **1985**, *82*, 270.
(17) Wang, P.; Zakeeruddin, S. M.; Comte, P.; Charvet, R.; Humphry-Baker, R.; Grätzel, M. *J. Phys. Chem. B* **2003**, *107*, 14336.

acetonitrile and drying by air flow, the sensitized titania electrodes were assembled with thermally platinized conducting glass electrodes. The electrodes were separated by a 25 μm thick Surlyn (or 35 μm thick Bynel) hot-melt gasket and sealed up by heating. The internal space was filled with a liquid electrolyte using a vacuum back filling system. The electrolyte-injecting hole made with a sand-blasting drill on the counter electrode glass substrate was sealed with a Bynel sheet and a thin glass cover by heating. Three electrolytes were used for device evaluations. Electrolyte A: 1.0 M DMII, 50 mM LiI, 30 mM I_2, 0.5 M *tert*-butylpyridine, and 0.1 M GNCS in the mixed solvent of acetonitrile and valeronitrile (v/v, 85/15); electrolyte B: 1.0 M DMII, 0.15 M I_2, 0.5 M NBB, and 0.1 M GNCS in MPN; electrolyte C: DMII/EMII/EMITCB/I_2/NBB/GNCS (molar ratio: 12/12/16/1.67/3.33/0.67). Devices A and B were made with electrolyte A, employing the C101 and C102 sensitizers, respectively. Device C was similar to device A, except that a 300 μM cheno in dye solution was used as coadsorbent during the staining process. Devices D and E were made with the C101 sensitizer in combination with electrolytes B and C, respectively.

Photovoltaic Characterization. A 450 W xenon light source (Oriel, U.S.A.) was used to give an irradiance of 100 mW cm^{-2} (the equivalent of one sun at air mass (AM) 1.5) at the surface of solar cells. The spectral output of the lamp was matched in the region of 350−750 nm with the aid of a Schott K113 Tempax sunlight filter (Präzisions Glas & Optik GmbH, Germany) so as to reduce the mismatch between the simulated and the true solar spectra. Various incident light intensities were regulated with wavelength neutral wire mesh attenuators. The current−voltage characteristics of the cell under these conditions were obtained by applying external potential bias to the cell and measuring the generated photocurrent with a Keithley model 2400 digital source meter (Keithley, U.S.A.). This process was fully automated using Wavemetrics software (http://www.wavemetrics.com/). A similar data acquisition system was used to control the incident photon-to-collected electron conversion efficiency measurement. Under full computer control, light from a 300 W xenon lamp (ILC Technology, U.S.A.) was focused through a Gemini-180 double monochromator (Jobin Yvon Ltd., U.K.) onto the photovoltaic cell under test. The monochromator was incremented through the visible spectrum to generate the IPCE (λ) as defined by IPCE (λ) = 12400(J_{sc}/$\lambda\phi$), where λ is the wavelength, J_{sc} is short-circuit photocurrent density (mA cm^{-2}), and ϕ is the incident radiative flux (mW cm^{-2}). Photovoltaic performance was measured by using a metal mask with an aperture area of 0.158 cm^2.

Transient Photoelectrical Measurements. In the transient photovoltage decay experiment, different steady-state lights were supplied with a homemade white light-emitting diode array by tuning the driving voltage, and a red light-emitting diode array controlled with a fast solid-state switch was used to generate a perturbation pulse with a width of 200 ms. The pulsed red- and steady-state white-lights were both incident on the photoanode side of a testing cell. The pulsed red lights were carefully controlled by the driving potential of the red diode array to keep the modulated photovoltages below 10 mV. We used red light as a probe to generate a photovoltage perturbation near the V_{oc} of the cell under the white light and measured the voltage decay process thereafter. Normally, the decay follows closely a monoexponential form, thus the recombination rate, k_r, can be extracted from the slope of the semilogarithmic plot. The capacitance of the TiO_2/electrolyte interface and DOS at the V_{oc} are calculated as $C_\mu = \Delta Q/\Delta V$, where ΔV is the peak of the photovoltage transient and ΔQ is the number of electron injected during the red light flash. The latter is obtained by integrating a short-circuit photocurrent transient generated from an identical red-light pulse. This method may underestimate the actual injected electrons by the fraction that is lost due to recombination during transport. The error is thought to be less than 30% in the worst case and, more critically, it will affect only the magnitude but not the shape of the calculated capacitance versus potential curves. The electron density in the titania film under a given white light intensity was measured by the charge extraction method.

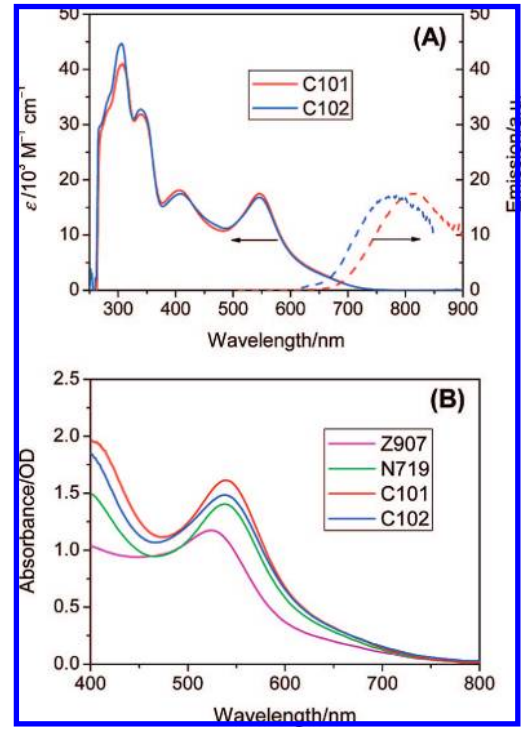

Figure 2. (A) Electronic absorption and emission spectra of C101 and C102 sensitizers in DMF. (B) Absorption spectra of Z907, N719, C101, and C102 anchored on a 7 μm thick transparent nanocrystalline TiO_2 film.

Electrical Impedance Measurements. Electrical impedance experiments were carried out with an Echo Chemie Autolab electrochemical workstation, with a frequency range of 0.01−10^6 Hz and a potential modulation of 5 mV. The obtained impedance spectra were fitted with the Z-view software (v2.8b, Scribner Associates Inc.) in terms of appropriate equivalent circuits.

Stability Tests. Solar cells covered with a 50 μm thick of polyester film (Preservation Equipment Ltd., U.K.) as a 400 nm UV cutoff filter were irradiated at open circuit under a Suntest CPS plus lamp (ATLAS GmbH, 100 mW cm^{-2}) in ambient air at 60 °C. Photoelectrochemical measurements were carried out at room temperature after allowing the cells to cool down and equilibrate during 2 h.

Results and Discussion

Electronic Absorption, Emission, and Redox Behavious. As shown in Figure 2, the intense absorption bands at 305 and 341 nm in the UV region are due to intraligand ($\pi\rightarrow\pi^*$) charge transitions of the dcbpy and conjugated ancillary ligands (L1 and L2). Also, the electronic absorption spectrum of C101 as well as C102 shows the characteristic metal-to-ligand charge-transfer transition (MLCT) absorption bands in the visible region like other heteroleptic polypyridyl ruthenium(II) complexes.[7,8] In DMF, these MLCT transition absorptions arise at ~407 and 547 nm, which are 23 nm red-shifted compared to that of Z907 or its analogues. The molar extinction coefficients (ε) of the low-energy MLCT absorption bands for C101 and C102 are 17.5 × 10^3 M^{-1} cm^{-1} and 16.8 × 10^3 M^{-1} cm^{-1}, respectively, which are significantly higher than the corresponding values

for the standard Z907 (12.2×10^3 M^{-1} cm^{-1}) and N719 (14.2×10^3 M^{-1} cm^{-1}) sensitizers.[18]

The calculated optical spectra shown in the Supporting Information, Figure S2, are in close agreement with experimental data, ensuring the correct assignments for different electronic transitions. The low energy transitions above 500 nm, with oscillator strength larger than 0.05 in both C101 and C102, are of MLCT characteristic. This can be viewed from the original (Supporting Information, Figures S3 and S5) and final states (Supporting Information, Figures S4 and S6) involved in the transitions. Detailed transition assignments for both C101 and C102 were summarized in Tables S1 and S2. We can see that in the MLCT transitions, the electrons delocalized over ruthenium and NCS are excited to final electronic states that mainly disperse on the bipyridyl ligands. The transition lead to a hole dispersed over NCS with a sizable population on the far end sulfur atom, giving a spatial convenience for dye regeneration.

The impressive improvements of extending the π-conjugated system of ancillary ligands in heteroleptic ruthenium complexes such as C101 and C102 complexes are apparent from Figure 2B, which depicts the absorption spectra in the visible region of Z907, N719, C101, and C102 anchored on a 7 μm thick transparent nanocrystalline TiO_2 film. Shortening of the light-absorption length of semiconducting film endowed by the C101 sensitizer is highly desirable to achieve a good charge collection yield for high efficiency DSCs. Also, the decrease of film thickness augments the open-circuit photovoltage of the cell due to lowering of the dark current.

As presented in Figure 2A, excitation of the low energy MLCT transitions of the C101 or C102 sensitizers in DMF produces an emission centered at 800 or 775 nm, respectively. The emission spectra were further analyzed by applying a Gaussian reconvolution method, which enabled to determine the integral under emission peak devoid of Raman and other instrumental artifacts.[19] The excitation transition energies (E_{0-0}) of C101 and C102 were estimated to be 1.60 and 1.61 eV. The redox potentials ($\phi^0(S^+/S)$) of the ruthenium center in C101 and C102 sensitizers determined by ultramicroelectrode square-wave voltammetry (see the Supporting Information, Figures S7 and S8) are 0.90 and 0.92 V versus NHE, which are 0.36 and 0.38 V higher than that of the iodide electron donor, providing an ample driving force for efficient dye regeneration, avoiding the geminate charge recombination. Furthermore, their excited-state formal redox potentials ($\phi^0(S^+/S^*)$) were calculated to be -0.70 and -0.69 V versus NHE. The negative offset of $\phi^0(S^+/S^*)$ relative to the conduction band edge of TiO_2 ensures the thermodynamic driving force for charge generation.

ATR-FTIR Spectra. The IR spectrum (Supporting Information, Figure S9) of C101 (or C102) anchored on TiO_2 film clearly shows the bands at 1609 (or 1614) cm^{-1} and 1383 cm^{-1} for the asymmetric and symmetric stretching modes of the carboxylate groups, indicating that the carboxylic acid is deprotonated and involved in the adsorption of the dye on the surface of TiO_2. From these ATR-FTIR data we can infer that the dye is anchored on the surface though the carboxylate group via a bidentate chelation or a bridging of surface titanium ions rather than an ester type linkage.[20] The sharp pyridine and thiophene (or furane) ring modes peak at 1541 cm^{-1}, 1429 cm^{-1}, 1231 cm^{-1}, and 1017 cm^{-1}. The NCS signal remains at 2102 cm^{-1}, indicating that NCS coordinated to the ruthenium center through the N atom is unaffected by the adsorption process. The saturated hydrocarbon chains of ancillary ligands are easily identified from their C−H stretch modes in the 2800−3000 cm^{-1} region. Peaks at 2852 and 2924 cm^{-1} are due to the symmetric and asymmetric $-CH_2-$ stretch vibrations. The corresponding CH_3- peak is observed at 2956 cm^{-1}, while the C−H stretching mode of aromatic rings is at 3070 cm^{-1}.

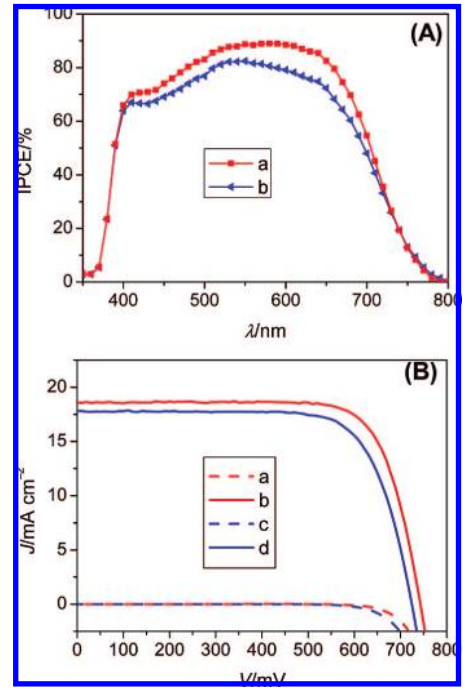

Figure 3. (A) Photocurrent action spectra: (a) device A; (b) device B. (B) $J-V$ characteristics measured under the irradiance of AM 1.5G sunlight of 100 mW cm^{-2} and in the dark: (a) device A in the dark; (b) device A under light; (c) device B in the dark; (d) device B under light. The electrolyte composition is as follows: 1.0 M DMII, 50 mM LiI, 30 mM I_2, 0.5 M *tert*-butylpyridine, and 0.1 M GNCS in the mixed solvent of acetonitrile and valeronitrile (*v*/*v*, 85/15).

Photovoltaic Performance and Device Stability. Figure 3A presents the typical photocurrent action spectra of devices A and B, employing an acetonitrile-based electrolyte, along with the corresponding C101 and C102 sensitizers, where the incident photon-to-collected electron conversion efficiency (IPCE) is plotted as a function of wavelength. The IPCE of C101 sensitizer exceeds 80% in the spectral region from 480 to 660 nm, reaching its maximum of 89% at 580 nm. Considering the light absorption and scattering loss by the conducting glass, the maximum efficiency for absorbed photon-to-collected electron conversion efficiency (APCE) is close to unity over a broad spectral range. In contrast, the C102 sensitizer has a relatively lower IPCE in the corresponding spectral region with a maximum of 82% at 550 nm, which could be partially correlated with the lower absorptivity of a mesoporous titania film anchored with C102 compared to that with C101. Figure 3B shows the current density−voltage characteristics of devices A and B at an irradiance of AM 1.5G full sunlight and in the dark. The short-circuit photocurrent density (J_{sc}), open-circuit photovoltage (V_{oc}),

(18) (a) Zakeeruddin, S. M.; Nazeeruddin, M. K.; Humphry-Baker, R.; Péchy, P.; Quagliotto, P.; Barolo, C.; Viscard, G.; Grätzel, M. *Langmuir* **2002**, *18*, 952. (b) Wang, P.; Wenger, B.; Humphry-Baker, R.; Moser, J.-E.; Teuscher, J.; Kantlehner, W.; Mezger, J.; Stoyanov, E. V.; Zakeeruddin, S. M.; Grätzel, M. *J. Am. Chem. Soc.* **2005**, *127*, 6850.

(19) Caspar, J. V.; Meyer, T. J. *J. Am. Chem. Soc.* **1983**, *105*, 5583.

(20) Shklover, V.; Ovehinnikov, Y. E.; Braginsky, L. S.; Zakeeruddin, S. M.; Grätzel, M. *Chem. Mater.* **1998**, *10*, 2533.

Table 1. Detailed Photovoltaic Parameters of a "Champion" DSC Made with C101 as Sensitizer and Cheno as Coadsorbent Measured under Different Incident Light Intensities[a]

P_{in}/mW cm^{-2}	J_{sc}/mA cm^{-2}	V_{oc}/mV	P_{max}/W m^{-2}	FF	η/%
29.72	5.42	746.2	33.7	0.833	11.3
51.17	9.27	761.0	57.4	0.813	11.2
64.42	11.65	765.9	71.7	0.804	11.1
99.39	17.94	777.7	109.5	0.785	11.0

[a] The spectral distribution of our measurement system simulates AM 1.5G solar emission. Incident power intensity, P_{in}; short-circuit photocurrent density, J_{sc}; open-circuit photovoltage, V_{oc}; maximum electricity output power density, P_{max}; fill factor, FF = P_{max}/P_{in}; and total power conversion efficiency, η. Cell area tested with a metal mask: 0.158 cm^2. The electrolyte composition is as follows: 1.0 M DMII, 50 mM LiI, 30 mM I_2, 0.5 M *tert*-butylpyridine, and 0.1 M GNCS in the mixed solvent of acetonitrile and valeronitrile (*v*/*v*, 85/15).

and fill factor (FF) of devices A are 18.62 mA cm^{-2}, 744 mV, and 0.755, respectively, yielding an overall conversion efficiency (η) of 10.5%. Consistent with the decrease of IPCE, the measured J_{sc} of 17.80 mA cm^{-2} for device B is also lower than that of device A; in addition, device B has a feature of lower V_{oc}, resulting in a lower power conversion efficiency of 9.5%. Considering the similar configuration, molecular size, and anchoring mode of the two sensitizers, we compared their ratios of molar extinction coefficients and the absorptivities of dye-coated titania films, deriving that C102 has a lower surface coverage than that of C101. This has been further confirmed by the dark current measurements. The more exposed surfaces directly contacted with an electrolyte will result in a fast recombination between triiodide and photoinjected electrons in the titania film, probably diminishing the charge collection yield. Apart from that a low J_{sc} produces a low V_{oc}, the more surface states below the conduction band edge due to the presence of more uncovered titania surfaces in the C102 case will also contribute to the measured low V_{oc} related to the quasi-fermi level of the mesoporous titania film under light.

Keeping in mind the importance of molecular-scale interface engineering,[5b,17] we employed cheno as a coadsorbent of C101 sensitizer at a molar ratio of 1/1 in the staining solution to improve the device efficiency. As shown in Figure S10, the photovoltaic parameters (J_{sc}, V_{oc}, FF, and η) of device C measured under the illumination of AM 1.5G full sunlight (99.39 mW cm^{-2}) are 17.94 mA cm^{-2}, 778 mV, 0.785, and 11.0%, respectively. Under various low light intensities, device efficiencies are even higher, up to 11.3%, as listed in Table 1. Obtaining such a high conversion efficiency with the C101 sensitizer by using a relatively thin double layer film (the transparent layer is just 7 μm) is impressive compared to a reference cell with the Z907 dye showing a ~9.0% efficiency. Note that a 12 μm thick titania film was used for a cell with the N719 sensitizer exhibiting an 11.18% conversion efficiency.[4a] Further efforts to make a DSC gathering the high J_{sc} of device A and high V_{oc} of device C together are underway to fully explore the maximal efficiency of this C101 sensitizer.

Due to the impossibility in sealing a highly volatile solvent such as acetonitrile for long-term thermal testing in our laboratories, a MPN-based electrolyte was used to evaluate the preliminary stability of the C101 sensitizer under moderate thermal stress and visible-light soaking. The feature of MPN lies in its high boiling point, low-volatility, nontoxicity, and good photochemical stability, making it viable for practical application apart from the need for robust encapsulation. As shown in Figure 4, under the standard AM 1.5G full sunlight, photovoltaic parameters (J_{sc}, V_{oc}, FF, and η) of device D using

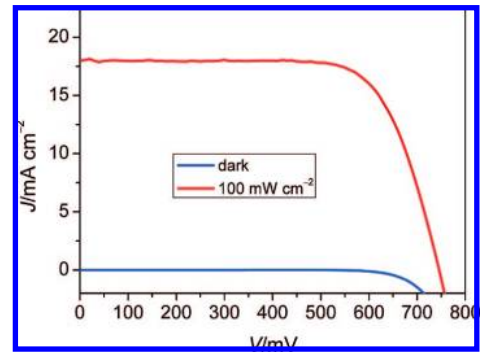

Figure 4. $J-V$ characteristics of device D measured in dark and under the irradiance of AM 1.5G sunlight of 100 mW cm^{-2}. The electrolyte composition is as follows: 1.0 M DMII, 0.15 M I_2, 0.5 M NBB, and 0.1 M GNCS in MPN.

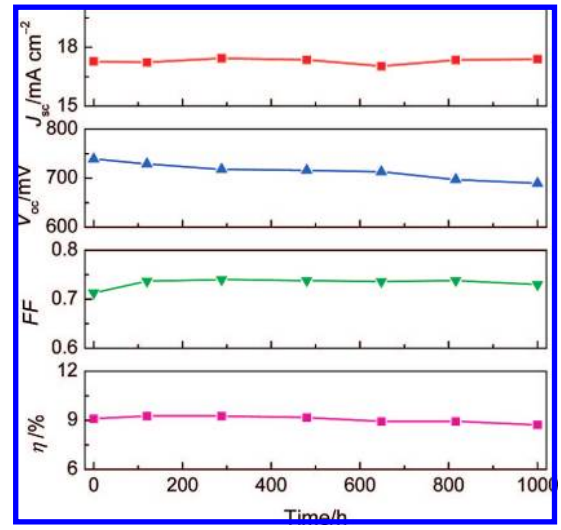

Figure 5. Detailed photovoltaic parameters of device D measured under the irradiance of AM 1.5G sunlight during successive one sun, visible light soaking at 60 °C.

the C101 sensitizer along with a low-volatility electrolyte are 17.98 mA cm^{-2}, 746 mV, 0.737, and 9.7%, respectively. Over 9% of this cell was retained over 96% of its initial performance (Figure 5) under both the thermal and the light-soaking stress for over 1000 h. This is the first time that such a high efficiency excitonic solar cell has passed a long-term stability testing. During the whole aging process, a small unwanted drop of 50 mV in open-circuit potential was noted. As we did not observe any change in the diffusion and redox overpotentials of electrolytes on the platinized counter electrode, the decrease of V_{oc} should be mainly related to the surface state variation of the mesoporous film, probably caused by protons in the electrolyte that slowly replace the surface adsorbed guaninium and imidazolium cations. The V_{oc} drop could be attenuated by our previously developed cografting protocol to improve the compactness of the hydrophobic monolayer on the titania surface.[5b] The enhancement of device fill factor and short-circuit current during the initial ~300 h aging is due to a faster dye regeneration rate[5a] and thus a decrease in charge transfer resistance at the interface between the dye-coated nanocrystals and electrolyte. This effect is probably due to improved self-organization of C101 molecules on the surface of titania nanocrystals during aging and electrolyte penetration into cavities containing adsorbed dye molecules, where the electrolyte was originally not able to access.

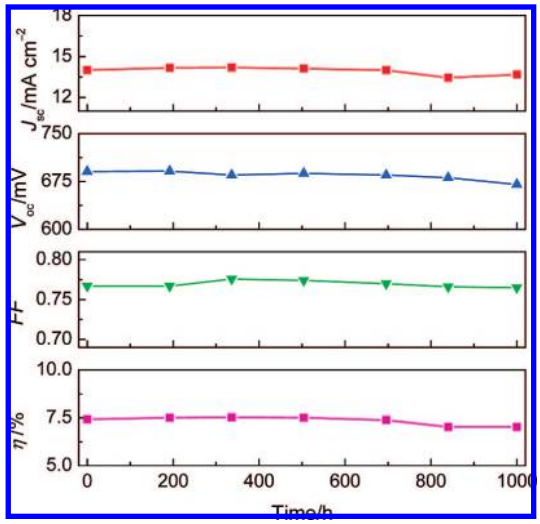

Figure 6. Detailed photovoltaic parameters of device E measured under the irradiance of AM 1.5G sunlight during successive one sun, visible-light soaking at 60 °C.

To lower the cost of photovoltaic power production a substantial improvement in device efficiency of DSCs is still desirable. Nevertheless, flexible and lightweight solar cells based on plastic matrix are attractive, even if their solar conversion efficiency is moderate, that is, in the 5−10% range. However, for these devices the use of organic solvents is prohibitive, as they would permeate across polymeric cell walls. A very attractive solution to this dilemma consists in employing ionic liquids as nonvolatile and thermally stable electrolytes.[18b,21] During the past years, solvent-free room temperature ionic liquid electrolytes of imidazolium melts have been actively pursued as a very attractive solution to this dilemma and over 7% efficiencies measured under AM 1.5G illumination have been achieved, but so far the device efficiencies of reported stable cells are lower than 7%.

For device E based on the C101 sensitizer employing a solvent-free, binary ionic liquid electrolyte, the corresponding device parameters (J_{sc}, V_{oc}, FF, and η) shown in Figure S11 are 14.77 mA cm^{-2}, 681 mV, 0.737, and 7.41%, respectively. As shown in Figure 6, device E demonstrated a very excellent light soaking stability at 60 °C. After 1000 h aging tests, device efficiency only changed from 7.41 to 7.04%. This is the first time that such a high efficiency DSC with solvent-free ionic liquid electrolytes has passed a long-term stability testing. This is expected to have an important practical consequence, as the use of solvents has impaired large-scale production and application of the flexible thin film DSCs.

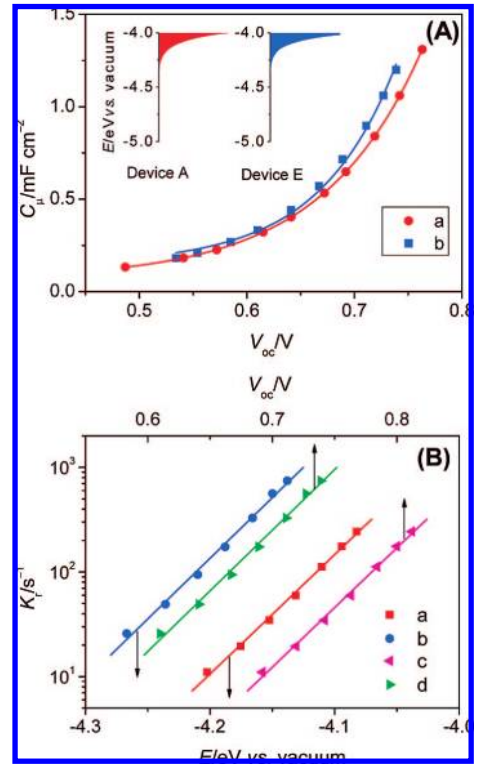

Figure 7. (A) Plots of chemical capacitances versus V_{oc}. The inset is the DOS profiles: (a) device A; (b) device E. (B) The dependence of recombination rate on V_{oc} or different energy levels of titania films: (a) and (c), device A; (b) and (d), device E.

Charge Transport, Recombination, and Collection. In the above discussion, we have highlighted the importance and urgency to develop stable and high-efficiency dye-sensitized solar cells with solvent-free electrolytes to facilitate their practical application. Apart from designing of more efficient sensitizers and mesoporous films and engineering of the titania/electrolyte nanointerface for further device enhancement, we are curious to understand the device physics of the relatively lower performance of device E compared with A. To scrutinize the origins of V_{oc} and J_{sc} differences between devices A and E, we first measured photovoltage transients[22] to have a close look on the charge recombination at the titania/electrolyte interface. As presented in Figure 7A, C_μ of devices A and E both arise exponentially with the increase of V_{oc}. As density of states (DOS), including surface and bulk traps, is proportional to C_μ, we have obtained exponential distributions of DOS for devices A and E shown in the inset of Figure 7A. Apparently, the surface states below the conduction band edge, due to the presence of unsaturated titanium species of the mesoporous titania film, have

(21) (a) Papageorgiou, N.; Athanassov, Y.; Armand, M.; Bonhôte, P.; Pettersson, H.; Azam, A.; Grätzel, M. *J. Electrochem. Soc.* **1996**, *143*, 3099. (b) Matsumoto, H.; Matsuda, T.; Tsuda, T.; Hagiwara, R.; Ito, Y.; Miyazaki, Y. *Chem. Lett.* **2001**, 26. (c) Kubo, W.; Kitamura, T.; Hanabusa, K.; Wada, Y.; Yanagida, S. *Chem. Commun.* **2002**, 374. (d) Wang, P.; Zakeeruddin, S. M.; Exnar, I.; Grätzel, M. *Chem. Commun.* **2002**, 2972. (e) Wang, P.; Zakeeruddin, S. M.; Comte, P.; Exnar, I.; Grätzel, M. *J. Am. Chem. Soc.* **2003**, *125*, 1166. (f) Wang, P.; Zakeeruddin, S. M.; Moser, J.-E.; Grätzel, M. *J. Phys. Chem. B* **2003**, *107*, 13280. (g) Wang, P.; Zakeeruddin, S. M.; Humphry-Baker, R.; Grätzel, M. *Chem. Mater.* **2004**, *16*, 2694. (h) Wang, P.; Zakeeruddin, S. M.; Moser, J.-E.; Humphry-Baker, R.; Grätzel, M. *J. Am. Chem. Soc.* **2004**, *126*, 7164. (i) Kuang, D.; Wang, P.; Ito, S.; Zakeeruddin, S. M.; Grätzel, M. *J. Am. Chem. Soc.* **2006**, *128*, 7732. (j) Kato, T.; Okazaki, A.; Hayase, S. *Chem. Commun.* **2005**, 363. (k) Zistler, M.; Wachter, P.; Schreiner, C.; Fleischmann, M.; Gerhard, D.; Wasserscheid, P.; Hinsch, A.; Goresa, H. J. *J. Electrochem. Soc.* **2007**, *154*, B925. (l) Gorlov, M.; Pettersson, H.; Hagfeldt, A.; Kloo, L. *Inorg. Chem.* **2007**, *46*, 3566. (m) Macfarlane, D. R.; Forsyth, M.; Howlett, P. C.; Pringle, J. M.; Sun, J.; Annat, G.; Neil, W.; Izgorodina, E. I. *Acc. Chem. Res.* **2007**, *40*, 1165. (n) Paulsson, H.; Hagfeldt, A.; Kloo, L. *J. Phys. Chem. B* **2003**, *107*, 13665.

(22) (a) O'Regan, B. C.; Lenzmann, F. *J. Phys. Chem. B* **2004**, *108*, 4342. (b) Bailes, M.; Cameron, P. J.; Lobato, K.; Peter, L. M. *J. Phys. Chem. B* **2005**, *109*, 15429. (c) Kopidakis, N.; Neale, N. R.; Frank, A. J. *J. Phys. Chem. B* **2006**, *110*, 12485. (d) Walker, A. B.; Peter, L. M.; Lobato, K.; Cameron, P. J. *J. Phys. Chem. B* **2006**, *110*, 25504. (e) Quintana, M.; Edvinsson, T.; Hagfeldt, A.; Boschloo, G. *J. Phys. Chem. C* **2007**, *111*, 1035. (f) Zhang, Z.; Zakeeruddin, S. M.; O'Regan, B. C.; Humphry-Baker, R.; Grätzel, M. *J. Phys. Chem. B* **2005**, *109*, 21818. (g) Zhang, Z.; Evans, N.; Zakeeruddin, S. M.; Humphry-Baker, R.; Grätzel, M. *J. Phys. Chem. C* **2007**, *111*, 398.

been partially passivated by guanidinium thiocyanate in device A, even with lithium ions inside. However, in device E with the solvent-free ionic liquid electrolyte guanidinium may not passivate titanium species very efficiently due to the extraordinarily high ion strength. This also indicates that TiO_2 nanocrystals are not fully covered by dye molecules and partially in contact with electrolytes. Furthermore, we have noted that the tetracyanoborate anion in ionic electrolytes does not have a strong interaction with TiO_2, different from the behavior of dicyanoamide used in our previous work.[21f] The uplifted conduction band-edge of sensitized titania film, positive-shifted equilibrium potential of electrolyte, and higher photocurrent density together explains the observed higher V_{oc} for device A in contrast to device E.

It is known that the charge recombination at the titania/electrolyte interface depends on the thermodynamic driving force as well as charge densities. The pseudo-first-order recombination rate (k_r) was determined from small perturbation photovoltage transient decays at different V_{oc}, by adjusting output light intensities of white light-emitting diodes. Figure 7B presents the semilogarithmic plot of k_r versus V_{oc} or the energy level of photoanodes (E versus vacuum). The linear fitting of all the data gave a similar slope value of 11.5 ± 0.1 for both devices A and E, indicative of a similar recombination mechanism in both devices. This slope corresponds to ~90 mV per decade, which is smaller than the values of 120 mV per decade obtained for solid-state DSCs.[22a] Obviously, along with increasing V_{oc} or up-lifting the energy levels of titania films, the recombination rates become higher due to the higher electron densities in the titania film as well as larger driving forces for charge recombination. If we just consider the same driving force for recombination by looking at the plot of k_r versus V_{oc}, it is clear that the logarithmic recombination rate ratio of device E to A is ~2. Note that even if there is not much difference in the DOS profiles of these two devices, at the same V_{oc}, device E has a higher electron density due to uplifting the equilibrium potential of its electrolyte relative to that of device A. Thus, we also compared the recombination rates at the same energy levels of titania films, while in this case the driving force of recombination is smaller for device E than A. Even though, the logarithmic k_r ratio is still ~1.9, as shown in Figure 7B. Thus, we believe that the faster recombination in the ionic liquid based device is mainly caused by the higher triiodide concentration of ~0.24 M compared to that of 0.03 M in device A. In addition, it is possible to have an even higher local concentration of triiodide close to photoanode in device E due to the low-fluidity of its electrolyte, enhancing the charge recombination at the titania/electrolyte interface.

We further resorted to the electrical impedance measurements[23] to clarify the charge transport in devices A and E with different electron densities in the titania film. As shown in Figure 8A, at the same DOS, device E always shows a feature of shorter electron lifetime, consistent with the above transient photovoltage decay measurements. Because there is not too much difference in the DOS profiles of device A and E, it is surprising to see the higher electron diffusion coefficient in device A compared to E in terms of the trapping-detrapping electron transport model in the titania film. Actually, this is in keeping

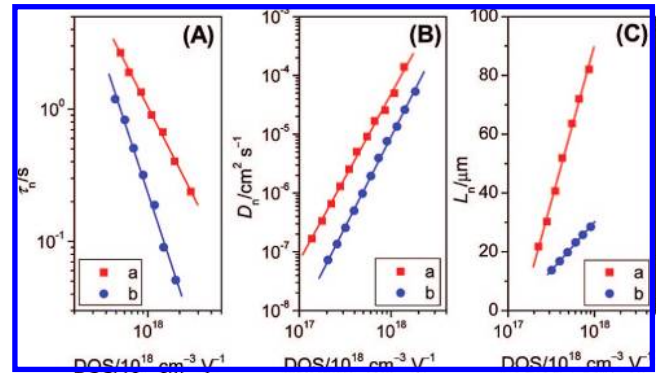

Figure 8. Plots of electron lifetime, diffusion coefficient, and diffusion length versus DOS: (a) device A; (b) device E.

with the notion[24] that the diffusion coefficient is ambipolar, reflecting apart from the electron motion also the diffusion of cations that screen the photoinjected electrons in the mesoporous titania film.[25] Although the total concentration of cations in device A is ~1.15 M compared with that of ~5.86 M in device E, the fluidity ratio of 184 for electrolyte A to C endows a much higher diffusion flux of cations in device A, efficiently speeding up the transport of electrons in the mesoporous titania film. The large electron diffusion length (L_n) directly related to a high charge collection yield is well consistent with the high J_{sc} observed for device A.

Conclusions

In summary, two new heteroleptic polypyridyl ruthenium complexes with high molar extinction coefficients have been synthesized and demonstrated as efficient sensitizers. The optical absorptivities of mesoporous titania film have been enhanced with these sensitizers by extending the π conjugated system of ancillary ligands. Shortening of the light-absorption length of semiconducting film endowed by these sensitizers are very important to achieve a good charge collection yield for high-efficiency dye-sensitized solar cells. On the basis of the new C101 sensitizer, several new DSC benchmarks under the illumination of AM 1.5G full sunlight have been reached, such as a 11.0% efficiency along with an acetonitrile based electrolyte, a long-term stable >9% device using a low volatility electrolyte, and a long-term stable ~7.4% device employing an ionic liquid electrolyte. We are now actively taking the advantage of the C101 sensitizer and its analogues for all-solid-sate dye-sensitized solar cells, where the conflict between light absorption length and charge diffusion length is even more serious.

Furthermore, we remark that, for the future efficiency enhancement of DSCs with solvent-free ionic liquid electrolytes by improving the charge collection yield, it is pertinent to considerably reduce the charge recombination and enhance the electron transport. This could be realized by reducing the viscosity of practical electrolyte systems, through which not only the diffusion coefficients of cations screening electrons in the titania film can be improved, but also the use of low triiodide concentration will be allowed without causing the mass transport limit of photocurrent. Also, the smart design of a more efficient sensitizer along with rational interface engineering such as

(23) (a) Bisquert, J. *J. Phys. Chem. B* **2002**, *106*, 325. (b) Bisquert, J. *Phys. Chem. Chem. Phys.* **2003**, *5*, 5360. (c) Bisquert, J. *Phys. Chem. Chem. Phys.* **2008**, *10*, 49.

(24) Kopidakis, N.; Schiff, E. A.; Park, N.-G.; van de Lagemaat, J.; Frank, A. J. *J. Phys. Chem. B* **2000**, *104*, 3930.

(25) Lanning, O. J.; Madden, P. *J. Phys. Chem. B* **2004**, *108*, 11069.

oxide-coating of titania nanocrystals[26] or pinhole-filling with coadsorbed small molecules or ions should make contribution to this issue.

Acknowledgment. We are grateful to P. Comte for the mesoporous titania film preparation. The National Key Scientific Program-Nanoscience and Nanotechnology (No. 2007CB936700), the National Science Foundation of China (50773078), the Science Foundation for Outstanding Young Scientists of Jilin Province (20070101), and the "100-Talent Program" of Chinese Academy of Sciences have supported this work. M.W., R. H.-B., S.M.Z., and M.G. thank the Swiss National Science Foundation for financial support.

Supporting Information Available: Additional calculation results, electronic transition assignments, and voltammetric data. This material is available free of charge via the Internet at http://pubs.acs.org.

JA801942J

(26) Palomares, E.; Clifford, J. N.; Haque, S. A.; Lutz, T.; Durrant, J. R. *J. Am. Chem. Soc.* **2003**, *125*, 475.